J Neurophysiol 100: 1835–1847, 2008.
First published July 30, 2008; doi:10.1152/jn.90261.2008.

Kv4 Accessory Protein DPPX (DPP6) is a Critical Regulator of Membrane Excitability in Hippocampal CA1 Pyramidal Neurons

Jinhyun Kim,[1,*] Marcela S. Nadal,[2,*] Ann M. Clemens,[1] Matthew Baron,[1] Sung-Cherl Jung,[1] Yoshio Misumi,[3] Bernardo Rudy,[2] and Dax A. Hoffman[1]

[1]*Molecular Neurophysiology and Biophysics Unit, Laboratory of Cellular and Synaptic Neurophysiology, National Institute of Child Health and Human Development, National Institutes of Health, Bethesda, Maryland;* [2]*Department of Physiology and Neuroscience Smilow Neuroscience Program, New York University School of Medicine, New York City, New York; and* [3]*Department of Cell Biology, School of Medicine, Fukuoka University, Fukuoka, Japan*

Submitted 11 February 2008; accepted in final form 23 July 2008

Kim J, Nadal MS, Clemens AM, Baron M, Jung S-C, Misumi Y, Rudy B, and Hoffman DA. Kv4 accessory protein DPPX is a critical regulator of membrane excitability in hippocampal CA1 pyramidal neurons. *J Neurophysiol* 100: 1835–1847, 2008. First published July 30, 2008; doi:10.1152/jn.90261.2008. A-type K^+ currents have unique kinetic and voltage-dependent properties that allow them to finely tune synaptic integration, action potential (AP) shape and firing patterns. In hippocampal CA1 pyramidal neurons, Kv4 channels make up the majority of the somatodendritic A-type current. Studies in heterologous expression systems have shown that Kv4 channels interact with transmembrane dipeptidyl-peptidase-like proteins (DPPLs) to regulate the surface trafficking and biophysical properties of Kv4 channels. To investigate the influence of DPPLs in a native system, we conducted voltage-clamp experiments in patches from CA1 pyramidal neurons expressing short-interfering RNA (siRNA) targeting the DPPL variant known to be expressed in hippocampal pyramidal neurons, DPPX (siDPPX). In accordance with heterologous studies, we found that DPPX downregulation in neurons resulted in depolarizing shifts of the steady-state inactivation and activation curves, a shallower conductance-voltage slope, slowed inactivation, and a delayed recovery from inactivation for A-type currents. We carried out current-clamp experiments to determine the physiological effect of the A-type current modifications by DPPX. Neurons expressing siDPPX exhibited a surprisingly large reduction in subthreshold excitability as measured by a decrease in input resistance, delayed time to AP onset, and an increased AP threshold. Suprathreshold DPPX downregulation resulted in slower AP rise and weaker repolarization. Computer simulations supported our experimental results and demonstrated how DPPX remodeling of A-channel properties can result in opposing sub- and suprathreshold effects on excitability. The Kv4 auxiliary subunit DPPX thus acts to increase neuronal responsiveness and enhance signal precision by advancing AP initiation and accelerating both the rise and repolarization of APs.

INTRODUCTION

Although it has been commonly thought that neurons represent information through mean firing rate, spike timing as an encoding mechanism has recently been observed in sensory systems (VanRullen et al. 2005). In the hippocampus too, the precision timing of action potentials (APs) is important for spike-timing-dependent plasticity and phase firing during theta oscillation. As the primary regulators of membrane excitability, voltage-gated potassium channels (Kv) thus play a fundamental role in the information processing of the hippocampus. Our previous studies have shown that subthreshold activating A-type K^+ currents contribute to spike initiation in hippocampal CA1 pyramidal neurons (Hoffman et al. 1997; Kim et al. 2005). In addition, these currents contribute to AP repolarization, modulate the frequency of repetitive firing, and have important roles in signal processing in dendrites (Connor and Stevens 1971; Hoffman et al. 1997; Johnston et al. 1999, 2000; Kim et al. 2005, 2007; Schoppa and Westbrook 1999). Any change in subcellular distribution of these channels or modulation of their kinetic/voltage-dependent properties could then have important consequences on dendritic integration and neuronal output.

Kv4.2 channel subunits are the predominant pore-forming subunits of somatodendritic A currents in hippocampal CA1 pyramidal neurons (Chen et al. 2006; Kim and Hoffman 2008; Kim et al. 2005; Lauver et al. 2006; Rhodes et al. 2004; Serodio and Rudy 1998). Studies in heterologous expression systems have shown that Kv4 proteins interact with at least two auxiliary subunits: Kv-channel-interacting proteins (KChIPs) and the dipeptidyl-peptidase-like proteins (DPPLs) DPPX (also known as DPP6) and DPP10 (An et al. 2000; Jerng et al. 2004a, 2005; Nadal et al. 2001, 2003; Ren et al. 2005; Zagha et al. 2005). Of these two, DPPX is the predominant DPPL in hippocampal pyramidal neurons (Zagha et al. 2005). DPPLs are single transmembrane proteins with a small intracellular N-terminus and a large extracellular C-terminal domain (Kin et al. 2001; Strop et al. 2004) that are prominently expressed in brain neuronal populations that also express Kv4 subunits (Jerng et al. 2007; Nadal et al. 2003, 2006; Zagha et al. 2005). When Kv4 subunits are co-expressed in heterologous systems with DPPX (a DPPIV-related DPPL lacking enzymatic activity), many properties of native A-type currents are restored, including a leftward shift of steady-state inactivation and activation curves and acceleration of recovery from inactivation, time to peak, and decay times (Nadal et al. 2003). Recently it has been shown that DPPX "tunes up" Kv4 channels by remodeling channel gating (Dougherty and Covarrubias 2006). The effects of this accessory subunit appear to occur through putative interactions between the voltage-sensing domain of Kv4.2 and the transmembrane segment of DPPX

* J. Kim and M. S. Nadal contributed equally to this work.

Address for reprint requests and other correspondence: D. A. Hoffman, Molecular Neurophysiology and Biophysics Unit, Laboratory of Cellular and Synaptic Neurophysiology, National Institute of Child Health and Human Development, National Institutes of Health, 35 Lincoln Dr., Rm. 3C-905, Bethesda, MD 20892-3715 (E-mail: hoffmand@mail.nih.gov).

The costs of publication of this article were defrayed in part by the payment of page charges. The article must therefore be hereby marked "*advertisement*" in accordance with 18 U.S.C. Section 1734 solely to indicate this fact.

or DPP10 (Ren et al. 2005; Zagha et al. 2005), altering the energy profile of the channel's voltage sensor.

To investigate the physiological role of DPPX in CA1 neurons, we developed short-interfering RNAs (siRNAs) to suppress the expression of all DPPX alternatively spliced variants. The efficacy of one of the DPPX-specific siRNAs (siDPPX) tested in Chinese hamster ovary (CHO) cells co-expressing Kv4.2 and the DPPX-S splice variant (from here on referred to as DPPX) was >95% complete as quantified by immunoblotting. To investigate whether DPPX alters the kinetics of A-type currents in a native system, we conducted voltage-clamp recordings from CA1 pyramidal neurons in hippocampal organotypic slices infected with siDPPX. As expected from studies co-expressing channel components in heterologous cells, we found that downregulation of DPPX resulted in a delayed recovery from inactivation, slowdown of activation and inactivation, and rightward shifts of the steady-state inactivation and activation curves for A-type currents. No significant changes in A-type current density were found, perhaps owing to the presence of endogenous KChIP proteins, which alone are capable of augmenting current density to levels that are seen with the DPPX, KChIP, Kv4 triple complex (Jerng et al. 2005). To determine the physiological effect of the A-type current kinetic modifications by DPPX, we carried out current-clamp experiments in siDPPX-expressing cells. Compared with negative control siRNA-expressing neurons, siDPPX-expressing neurons exhibited changes in cellular input resistance, time to AP onset, AP rise time and repolarization, and early firing frequency. NEURON computer simulations linked these changes to a siDPPX-mediated depolarizing shift of the inactivation curve of the A current and a shallowing of the activation curve slope, enhancing subthreshold A-current activity levels. Suprathreshold siDPPX had the opposite effect, enhancing excitability by decreasing A-current activity through a depolarizing shift in the voltage dependence to activation. Together these results suggest that DPPX acts natively to boost neuronal response by decreasing time to first spike onset and to enhance signal precision by sharpening both the rising and falling phase of APs. DPPX co-expression in the CA1 neurons is therefore an important contributor to spike-time-dependent information coding.

METHODS

Construction of siRNAs

For siRNA construction, we used the mammalian expression vector pSUPER containing H1 promoter (a generous gift from Dr. Reuven Agami, The Netherlands Cancer Institute). Three 19-nt rat DPPX-specific sequences (GenBank Accession No. M76427; *X309*: 5′CTGGAAAGGAATCGCCATT3′, *X320*: 5′TCGCCATTGCACTGCTTGT3′, *X2498*: 5′ GTCACTACTTTCACAGCGT3′) were used to design the hairpin siRNA template oligonucleotides (64-nt). The DPPX-specific 19-nt sequences of pSUPER-X309 and pSUPER-X320 starts 91 and 102 bp downstream of the starting codon of DPPX-S (M76427), respectively, and thus these two siRNAs have partially overlapping sequences (42%). That of pSUPER-X2498 starts 130 bp upstream the stop codon of the same DPPX gene. The choice of the sequences was guided by reported design strategies (Jagla et al. 2005) and the instructions accompanying the vector: the 19-nt sequence was flanked by two adenines at the 5′ and have GC richness of 47% for pSUPER- X309 and pSUPER-X2498 and 52% for pSUPER-X320.

The 64-nt oligonucleotides were purchased from Sigma Genosys, annealed in annealing buffer (100 mM K^+ acetate, 30 mM HEPES-K pH 7.4 and 2 mM Mg^{2+} Acetate), phosphorylated with T4 polynucleotide kinase (Roche, Indianapolis, IN) inserted into the pSUPER vector via *Bgl*II/*Hin*dIII, and confirmed by sequencing. CHO-K1 cells (American Type Culture Collection, Manassas, VA) were cultured in DMEM supplemented with 10% fetal calf serum and Glutamax (Invitrogen, Carlsbad, CA). CHO cells at 80% confluence in 6-cm plates were transfected with 1 μg of DPPX-S cDNA and 0.5 μg of Kv4.2 cDNA along with 1 μg of pSUPER-X309, pSUPER-X320, pSUPER-X2498 DPPX or pSUPER alone by using the transfection reagent FuGENE 6 (Roche) in accordance with manufacturer's protocol. To monitor transfection efficiency and label transfected cells for electrophysiological recordings, green fluorescent protein (pEGFP-C3, Clontech, Mountain View, CA) was co-transfected at a ratio 1:20. CHO cells were analyzed 48 h after transfection except as otherwise indicated. When different amounts of pSUPER-X309 were transfected, the total amount of siRNA vector was leveled to 3 μg by adding complementary amounts of pSUPER.

Viral expression of siRNAs in hippocampal neurons

For neuronal expression, the X309 DPPX with H1 promoter from pSUPER-X309 was amplified by PCR and subcloned into the attenuated Sindbis viral vector SINrep(nsP2S^{726})EGdsp, including EGFP under a separate subgenomic promoter and polyadenylation signal (illustrated in Supplemental Fig. S3[1]), through *Xba*I/*Pml*I. As a negative control, a nontargeting siRNA (Ambion, Austin, TX) was inserted into SINrep(nsP2S^{726})EGdsp as the X309. These constructs were prepared with the helper plasmid DH-BB(tRNA/TE12) as previously described (Kim et al. 2004). Hippocampal dissociated neurons were prepared and cultured as described previously (Kim et al. 2005). Neurons [12−14 day in vitro (DIV)] were infected with Sindbis virus (1–5 μl) up to ~50% of neurons, and infection rate was estimated by counting GFP-positive (infected) versus DAPI-counterlabeled (total) cells from different microscopic fields.

Immunoblot and quantitative analysis

Whole cell extracts from transfected CHO cells or infected hippocampal primary neurons were prepared in the presence of TNEE +1% Triton X-100 + protease inhibitors (Sigma, St. Louis, MO) at 4°C and 30 μg of total protein was separated on 10% SDS-polyacrilamide gel electrophoresis. Immunoblots were probed with antibodies against DPPX (Kin et al. 2001) (1:500), GFP (a gift from Dr. Ed Ziff, NYU School of Medicine, 1:500, Abgent, 1:2,000), HCN1 and HCN2 (a kind gift from Dr. Chetkovich, Northwestern University, 1:1,000), Kv1.2 and Kv1.4 (NeuroMab, 1:1,000) or β-Actin (Sigma, 1:1000) detected using enhanced chemiluminescence (ECL). Quantification was performed with ImageJ v1.40 (http://rsb.info.nih.gov/ij/).

CHO whole cell voltage-clamp recordings

CHO whole cell voltage clamp recordings were obtained with coverslips placed on a recording chamber on the stage of an inverted microscope using an Axopatch 200A amplifier (Molecular Devices, Sunnyvale, CA). Patch pipettes with 2– 4 MΩ resistance were filled with intracellular solution containing (in mM) 144 Kgluconate, 0.2 EGTA, 3 $MgCl_2$, 10 HEPES, 4 MgATP, and 0.5 NaGTP (pH adjusted to 7.4 with KOH). The extracellular solution contained (in mM) 135 NaCl, 3.5 KCl, 1.8 $CaCl_2$, 2 $MgCl_2$, 10 glucose, and 10 HEPES (pH adjusted to 7.3 with NaOH). Seal resistance was typically >2 GΩ. Currents were low-pass- filtered at 2 kHz and digitized at 2.5 kHz. Data acquisition and analysis was performed using Clampex Version 8 software (Molecular Devices). Step depolarizations between −90 and 40 mV at 10-mV intervals were applied from a holding potential of −70 mV followed by a 1 s hyperpolarizing prepulse to −100 mV.

[1] The online version of this article contains supplemental data.

Voltages were corrected for junction potential, which was calculated using Clampex Junction Potential Calculator software and gave a value of 10 mV. All recordings were carried out at room temperature (20–22°C).

Organotypic slice culture recordings

Hippocampal organotypic slice cultures (250 μm thick) were prepared as in Kim et al. 2005. On DIV 4, slices were infected with a normalized infectious titer of Sindbis virus carrying siDPPX (X309) or the negative control siRNA. For all electrophysiological recordings, organotypic slice cultures 1–3 days after infection were transferred to a submerged recording chamber with continuous flow of artificial cerebrospinal fluid (ACSF) containing (in mM): 125 NaCl, 25 $NaHCO_3$, 2.5 KCl, 1.25 NaH_2PO4, 2 $CaCl_2$, 1 $MgCl_2$, and 25 D-glucose bubbled with 5% CO_2-95% O_2. Hippocampal CA1 pyramidal neurons were identified using infrared differential interference contrast (IR-DIC) videomicroscopy. The patch electrodes (3–6 MΩ) were filled with (in mM): 125 Kgluconate, 20 KCl, 10 HEPES, 4 NaCl, 0.5 EGTA, 10 Na_2phosphocreatine, 4 ATP-Mg, 0.3 $Tris_2$GTP (pH 7.2 with KOH). Recordings were low-pass filtered at 2–5 kHz for voltage-clamp recordings and digitized at 10 kHz by an Instrutech ITC-18 A/D board controlled by software written for Igor Pro (WaveMetrics, Lake Oswego, OR).

Whole cell current-clamp recordings were made using a Multiclamp 700B amplifier (Molecular Devices) at 32–34°C. Series resistance was kept <19 MΩ. Voltages have not been corrected for junction potentials. Recordings of voltage-gated currents were made in voltage-clamp mode using an Axopatch-200B (Molecular Devices) or Multiclamp 700B amplifier at room temperature. Electrodes were pulled from borosilicate glass and in some experiments coated with silicone elastomer (Sylgard; Dow Corning) to reduce their capacitance. Current ensemble averages were constructed from 3 to 30 individual sweeps. Leakage and capacitive currents were subtracted digitally using either a P/5 protocol or null traces. The transient current was isolated from the sustained current using a 150-ms prepulse step to –20 mV to inactivate transient channels. All curve fits (inactivation time constants, Boltzmann fits and various *x-y* plots) were performed with a least-squares program (Igor Pro). TTX (1 μM, Sigma) was present in all (whole cell and outside-out patch) voltage-clamp experiments to block sodium currents. ZD288 was purchased from Tocris. For whole cell voltage-clamp experiments, series resistance was compensated to 85% and only recordings with <13 MΩ series resistance were included in the analysis.

Data analysis

Data analysis was performed using Igor Pro and Microsoft Excel (Microsoft, Redmond, WA). Numeric values are given as means ± SE. Error bars in the figures represent SE. Statistical significance was examined with Student's *t*-test or one-way ANOVA. For current-clamp analyses, the numeric value (AP threshold, width etc.) was typically taken as the average of three measurements from each cell. Unless otherwise stated, the data were taken from the first AP initiated on current injection. Where noted, control data from uninfected and negative control siRNA-expressing neurons showing no significant differences were pooled.

NEURON simulations

Our simulations were written in the NEURON programming environment (version 5.8) (Hines and Carnevale 1997) on a Dell Dimension 8300 series computer (Dell, Round Rock, TX) with a Pentium 4 processor running Windows XP Professional version 2002. A reconstructed CA1 pyramidal neuron, borrowed from a previous simulation (Magee and Cook 2000) was modeled in NEURON using one compartment for the soma and 412 compartments for the dendrites. An intracellular resistivity of R_a = 150 Ω-cm, a membrane time constant of τ_m = 28 ms (R_m = 28 kΩ-cm^2 and C_m = 1 μF/cm^2), and a membrane resting potential of V_{rest} = −65 mV were used. To account for spines and smaller dendritic branches that were not explicitly modeled, C_m was increased and R_m decreased each by a factor of 2 in the dendrites (Holmes 1989).

For channel kinetics, we implemented equations for three types of voltage-gated conductances with Hodgkin-Huxley-like gating: a Na^+ conductance, a fast A-type K^+ conductance, and a slow delayed-rectifier K^+ conductance, in addition to including a nonvoltage-gated leak conductance. These kinetic equations were based on those from a previous simulation (Migliore et al. 1999). As in this previous simulation, Na^+ peak conductance density was constant at 80 mS/cm^2 throughout the soma and dendrites, and the gating kinetics consisted of three independent gates: an activation gate (m), an inactivation gate (h), and a slow inactivation gate (s) to account for the slow inactivation of dendritic Na^+ channels experimentally observed in hippocampal CA1 pyramidal neurons (Colbert et al. 1997; Jung et al. 1997). Consistent with experimental findings (Hoffman et al. 1997) and previous simulation (Migliore et al. 1999), peak conductance density of A-type K^+ channels was set to 14.4 mS/cm^2 in the soma and linearly increased in the dendrites, with a peak conductance density given by the equation (1 + *d*/100) * 8.4 mS/cm^2, where *d* is the distance (in μm) from the soma, up to a maximum distance of 200 μm from the soma. For dendritic compartments >200 μm distance from the soma, A-type K^+ peak conductance density was constant at 14.4 mS/cm^2. The kinetic equations for delayed-rectifier K^+ conductance, a noninactivating voltage-gated K^+ conductance, were borrowed from a previous simulation (Migliore et al. 1999) and consistent with experimental observation (Hoffman et al. 1997). These channels were distributed throughout the soma and dendrites with a peak conductance density of 28 mS/cm^2.

RESULTS

Efficiency and specificity of siDPPX

There are five known alternatively spliced products of the DPPX gene: DPPX-S, DPPX-L, DPPX-K, DPPX-E, and DPPX-D, which are divergent at the N- terminus (Nadal et al. 2006). We designed three siRNAs targeting different regions of the DPPX coding sequence that is *common* to all splice variants. Each siRNA consisted of a sense 19-nt sequence derived from the DPPX transcript (see METHODS), separated by a short spacer from the reverse complement of the same 19-nt sequence, such that the resulting transcript forms a stem-loop structure (Brummelkamp et al. 2002). Supplemental Fig. S1*A* shows diagrams of the predicted secondary structures of the three siRNAs pSUPER-X309, pSUPER-X320, and pSUPER-X2498. A BLAST search against GenBank databases gave no similarities for any of the selected sequences.

Co-expression at a 1:1 ratio of DPPX-S and pSUPER-X309 in CHO cells nearly completely eliminated DPPX protein expression, whereas co-expression with pSUPER-X320 showed no elimination and co-expression with pSUPER-X2498 only produced partial elimination (Fig. 1*A*). No DPPX band was detected in the lane containing the extract from cells co-expressing pSUPER-X309. A very faint band was observed if a film from the same gel was overexposed. Quantification of this band suggests that pSUPER-X309 produced a >96% reduction in the levels of DPPX protein compared with protein levels in cells co-transfected with the empty vector pSUPER. The partially overlapping targeting sequence of pSUPER-X320 did not affect DPPX protein levels and pSUPER-X2498 suppressed

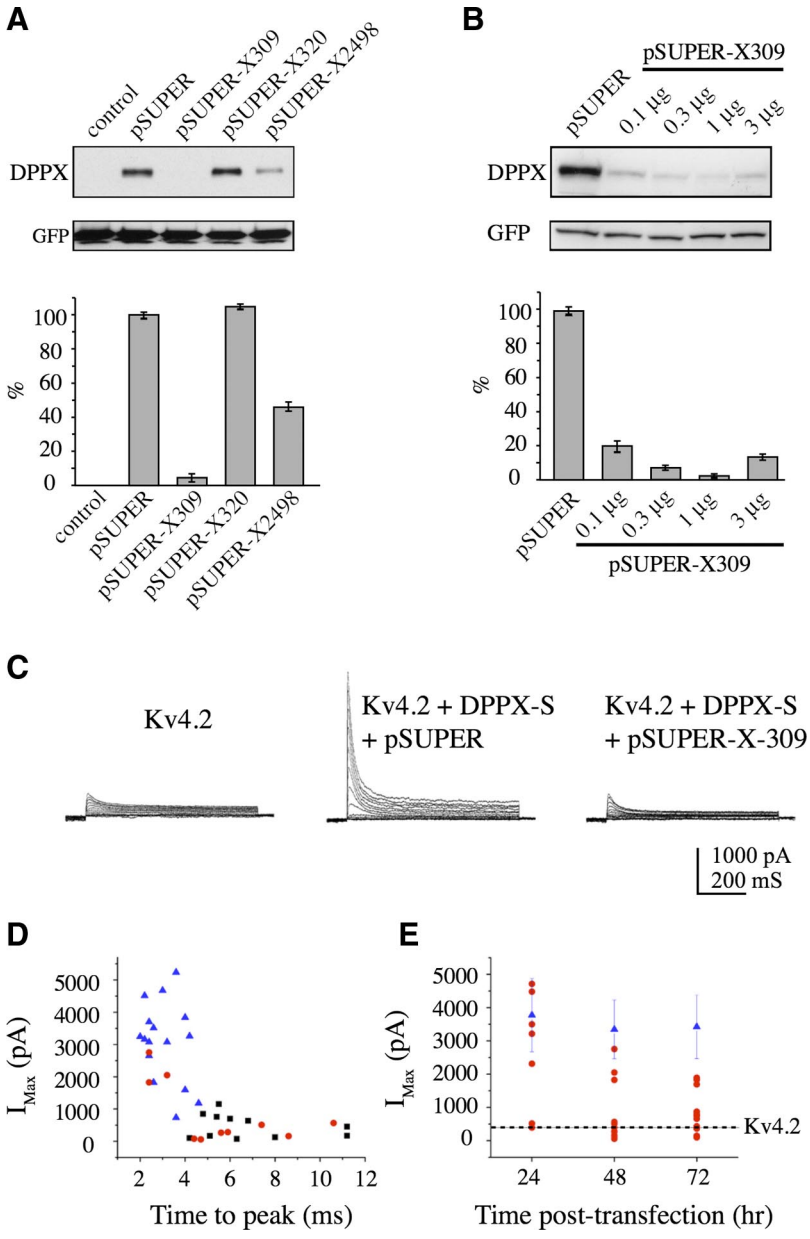

FIG. 1. Efficiency of dipeptidyl-peptidase-like protein (DPPL) DPPX knockdown by short-interfering RNAs (siRNAs). *A*: immunoblot analysis of CHO cells transfected with siRNAs or empty vector (pSUPER) at a 1:1 ratio with respect to DPPX-S cDNA. Control: cells transfected only with green fluorescent protein (GFP). Cells were harvested at 48 h post-transfection. The bar plots show the fraction of DPPX protein obtained from quantification of immunoblots after subtracting the background obtained from the control lane with respect to the value obtained in cells co-transfected with empty vector (100%). *B*: high sensitivity of X309 short-interfering DPPX (siDPPX) was shown by immunoblot analysis of CHO cells transfected with the increasing amounts of pSUPER-X309. The total amount of siRNA vector was kept constant at 3 μg by adding complementary amounts of empty pSUPER. Cells were harvested at 48 h posttransfection. *C*: examples of traces obtained at different voltages (see METHODS for voltage protocol) from CHO cells transfected with Kv4.2 cRNA alone (*left*), Kv4.2 + DPPX-S + pSUPER (*center*), and Kv4.2 + DPPX-S + pSUPER-X309 (*right*). *D*: peak current at +40 mV (I_{max}) plotted against time to peak during a depolarization to +40 mV in cells transfected with Kv4.2 alone (black squares), Kv4.2 + DPPX-S + pSUPER (blue triangles), or Kv4.2 + DPPX-S + pSUPER-X309 (red circles). *E*: current magnitudes recorded at 24, 48, and 72 h after transfection. Shown as blue triangles are averages (±SE) from cells transfected with Kv4.2 + DPPX-S + pSUPER at 24 h (n = 8), 48 hs (n = 16), and 72 h (n = 7). The dotted line represents the mean value for cells transfected with Kv4.2 alone (471.9 + 111.6, n = 11), which did not vary significantly with time after transfection. The red circles are individual cells transfected with Kv4.2 + DPPX-S + pSUPER-X309. Error bars represent SE.

DPPX expression by 55%, compared with the empty vector control.

In our tests, maximal DPPX silencing was observed when the ratio of co-transfected cDNAs was 1:1 (1 μg of pSUPER-X309 and 1 μg of DPPX-S, Fig. 1*B*). Increasing the amount of transfected pSUPER-X309 to 3 μg (1:3 ratio with respect to the DPPX-S cDNA) not only did not enhance the specific silencing effects but it had slight negative effects (Fig. 1*B*). Decreasing the amount of the siRNA vector 10 times (to 0.1 μg) did not reduce considerably the silencing effect (80% compared with 97% with 1 μg, Fig. 1*B*), even though there was now ten times less siRNA cDNA with respect to DPPX-S cDNA (0.1:1 ratio).

We also examined the time dependence of the ability of siRNA X309 to suppress DPPX expression (Supplemental Fig. S1*B*). CHO cells co-transfected with pSUPER-X309 and DPPX-S cDNAs at a 1:1 ratio were harvested and processed for Western blot analysis at 24, 48, and 72 h. The expression of DPPX-S protein reached a peak at 24 h, decreasing substantially at 72 h. In the groups of cells co-transfected with pSUPER-X309, DPPX-S expression was reduced by 84.4% at 24 h, 95.1% at 48 h, and 92.6% at 72 h compared with the respective controls. Thus the relative suppressive effect of the siRNA X-309 was already observed at 24 h; reached a maximum at 48 h and continued at high efficacy at 72 h in spite of the decrease in overall protein expression, as evidenced by weakened GFP signal at 72 h.

To determine the specificity of siRNA X309, we co-transfected pSUPER-X309 together with the cDNAs of another DPPX splice variant, DPPX-L, or the closely related dipeptidyl peptidase DPP10 (Supplemental Fig. S1*C*). Phylogenetic analysis showed that DPP10 and DPPX form an evolutionarily divergent subfamily within the extended DPPIV-like family (Qi et al. 2003; Zagha et al. 2005). The DPP10 amino acid sequence shares 51% identity with DPPX (Qi et al. 2003) and is especially similar in the juxtamembrane and transmembrane

regions, where they show 92% similarity (Zagha et al. 2005). Because the target sequence of DPPX siRNA X309 is located in the juxtamembrane region of DPPX, DPP10 is an ideal control for testing the specificity of this siRNA. pSUPER-X309 efficiently eliminated DPPX expression from DPPX-L transfected cells, resembling its effects on DPPX-S transfected cells but failed to suppress DPP10 expression, demonstrating that the pSUPER-X309 siRNA specifically targets DPPX.

Next we examined if the suppression of the expression of DPPX protein by the presence of DPPX siRNA X309 abolished the effects of DPPX on Kv4.2-mediated A-currents. As we have previously reported, DPPX-S has large effects on current magnitude and channel kinetics when co-expressed with Kv4.2 subunits both in *Xenopus* oocytes and in CHO cells (Nadal et al. 2003; Zagha et al. 2005) (Fig. 1*C, center*), compared with Kv4.2 alone (Fig. 1*C, left*). Co-transfection of pSUPER-X309 with Kv4.2 and DPPX-S inhibited the modulatory effect of DPPX-S on Kv4 currents in most cells analyzed (Fig. 1, *C, right, D,* and *E*). We analyzed three independent parameters that are notably affected by the presence of DPPX in the Kv4-channel complex: current magnitude, time to peak, and the voltage-dependence of activation. All three parameters were returned to the levels seen in cells expressing Kv4.2 alone in most cells co-transfected with pSUPER-X309 (Figs. 1*D* and Supplemental S2). Some siRNA X309-expressing cells (27.3%) had current levels and times to peak significantly higher than cells expressing Kv4.2 alone. Inhibition of the functional effects of DPPX by the siRNA, was weak 24 h after transfection but was robust at 48 and 72 h (Fig. 1*E*).

Effects of DPPX knockdown on native A-type K^+ currents in CA1 pyramidal neurons

To test the ability of siRNA X309 (siDPPX) to suppress endogenous DPPX expression in neurons, we used a modified Sindbis virus system (Kim et al. 2004, 2005). In this system, infected neurons express both of siDPPX and EGFP via the viral construct illustrated in Supplemental Fig. S3. In dissociated hippocampal cultures, ~50% of neurons showed EGFP fluorescence 2 days after infection. The immunoblot of extracts from these cultures shows siDPPX reduced endogenous DPPX by ~50% (Fig. 2*A*) of total, suggesting that, given ~50% efficiency in infection, endogenous DPPX is nearly eliminated by siDPPX expression in expressing neurons. Effective DPPX

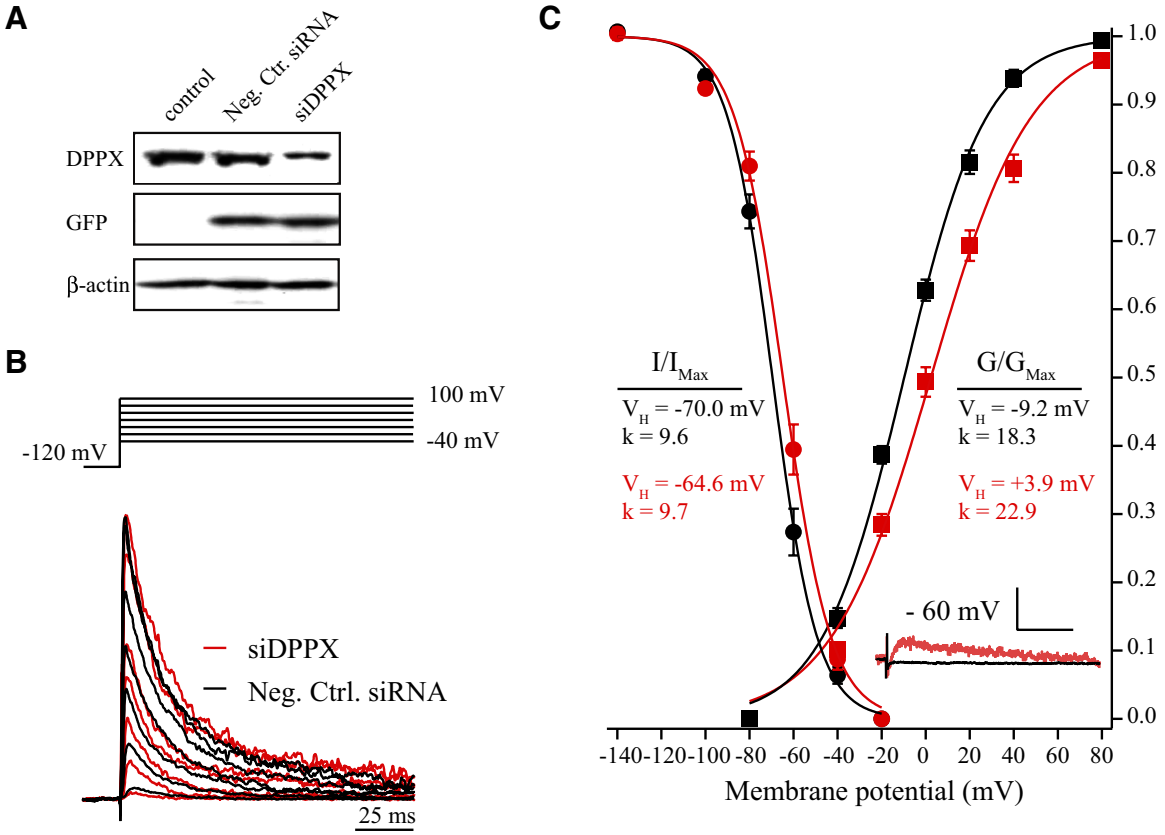

FIG. 2. Effects of siDPPX on A-type K^+-channel voltage-dependent properties in CA1 pyramidal neurons. *A*: efficiency of endogenous DPPX knockdown by siDPPX in hippocampal neurons. Immunoblots of hippocampal neurons (DIV 14), ~50% infected by the attenuated Sindbis virus-expressing siDPPX or negative control siRNA. The blots show that endogenous DPPX protein is substantially reduced by siDPPX within 2 days after infection, consistent with heterologous CHO cell data. β-actin is shown as control. *B*: representative traces from outside-out patches from siDPPX (red traces) and Neg. Ctrl. siRNA (black traces)-expressing neurons, scaled to the same peak amplitude for comparison. Voltage steps are depicted above. *C*: conductance voltage (G/G_{max}) and steady-state inactivation (I/I_{max}) curves for A-type currents recorded from somatic outside-out patches in siDPPX (days ^{2,3}, red circles and fits) and negative control siRNA (black circles and fits)-infected CA1 neurons. There was a rightward shift and significant change in slope for the steady-state activation curve. A rightward shift was also seen in the steady-state inactivation curve with siDPPX with no change in slope. *Inset*: traces are from whole cell recordings for a step from −120 to −60 mV. Neurons expressing siDPPX have larger currents at −60 mV than negative control siRNA-expressing neurons, consistent with the change in activation curve slope and inactivation curve shift. Subtraction artifacts are clipped for presentation. Scale bars: 50 pA, 100 ms. Error bars represent SE.

silencing lasted ≤72 h after infection (Supplemental Fig. S3). Viral expression of negative control siRNA had no effect on DPPX expression (Fig. 2*A*). It is also important to note that no significant silencing effects of siDPPX on other endogenous voltage-gated channels (HCN1, HCN2, Kv1.2, and Kv1.4) were detected (Supplemental Fig. S3).

To investigate the functional consequences of DPPX knockdown and to examine the physiological role of DPPX in neurons, we expressed siDPPX in CA1 hippocampal neurons in organotypic slice cultures. We chose to do the experiments in organotypic slice cultures because this is a more native preparation and is more adequate to study the effects of DPPX knockdown on neuronal excitability. Recordings from siDPPX-expressing neurons were compared with control (either uninfected or those infected with a negative control siRNA). Infected neurons from the two groups were not visually different and whole cell recordings revealed no significant difference in resting membrane potential or whole cell capacitance between groups (data not shown).

Outside-out patch-clamp recordings from CA1 hippocampal neurons, in the presence of TTX to block voltage-gated Na^+ channels, showed a large outward current composed of a rapidly inactivating component along with a sustained or slowly inactivating component. The transient current was isolated from the sustained current using a prepulse voltage protocol (METHODS). Patches pulled from neurons expressing siDPPX showed similar peak transient and sustained outward current densities compared with siRNA control neurons (Table 1). However, expressing siDPPX resulted in a significant rightward shift in both the activation and steady-state inactivation curves for transient currents (Fig. 2, *B* and *C,* Table 1, $P < 0.05$), consistent with the effects of DPPX on Kv4-mediated currents in heterologous systems (Jerng et al. 2004a,b; Nadal et al. 2003; Zagha et al. 2005).

In the heterologous expression studies, DPPX produced a significantly larger shift in the voltage dependence of activation compared with the effects on inactivation voltage-dependence. Likewise, siDPPX had a larger effect on the activation curve than on inactivation as shown in Fig. 2. However, we also found a significant change in the slope of the transient current activation curve after siDPPX expression (from 18.3 in control to 22.9 for siDPPX-expressing neurons, Fig. 2*C,* Table 1, $P < 0.05$) but not in the slope of the inactivation curve (9.4 in control vs. 9.6 in siDPPX-expressing neurons). Although an effect of DPPX on the slope of the conductance-voltage curve was not been highlighted in papers reporting results from heterologous expression systems, this effect was clearly present in those studies (cf. Table 1 in Nadal et al. 2003; Fig. 5 in Jerng et al. 2005; Table 1 in Nadal et al. 2006). Our experimental observations on CA1 neuron excitability and computer simulations indicate that this is an extremely important effect of DPPX.

Boltzmann fits to the data in Fig. 2*C* suggest that this slope change, along with the depolarizing inactivation curve shift, results in a *larger* window current in siDPPX-expressing neurons despite the positive shift in the conductance-voltage curve. We confirmed an enhanced window current in siDPPX expressing by measuring whole cell A currents near the resting potential in these neurons (−60 mV; 15.9 ± 5.8 pA, $n = 10$ for siDPPX vs. 5.1 ± 0.4 pA, $n = 13$ for negative controls siRNA, $P < 0.05$; Fig. 2*C, inset*). These measurements utilized whole

TABLE 1. *Expression level, voltage dependence, and kinetic properties of K^+ currents in outside-out patch recordings from CA1 neurons of organotypic slice cultures DIV 5–8*

	Current Density (pA/patch)		Activation		Inactivation		τ_{inact}, ms		τ_{recov}, ms
	Transient	Sustained	V_h	k	V_h	k	−20 mV	+40 mV	−100 mV
Control†	194 ± 22 (35)	44 ± 06 (35)	−9.2 ± 2.3 (34)	18.3 ± 0.7 (34)	−70.0 ± 1.1 (26)	9.6 ± 0.6 (26)	20.1 ± 1.7 (24)	33.9 ± 3.7 (23)	19.0 ± 1.5 (26)
siDPPX (days 2–3)	211 ± 21 (55)	66 ± 08 (55)	3.9 ± 2.0* (28)	22.9 ± 0.9* (28)	−64.6 ± 1.1* (36)	9.7 ± 0.4 (36)	29.6 ± 3.7* (26)	31.1 ± 2.9 (26)	31.8 ± 6.6* (12)#

†Control group includes recordings from 15 uninfected neurons and 20 infected with negative control siRNA numbers are in parentheses. V_h, k, average fit half-activation and inactivation voltages and slope; τ_{inact}, weighted sum of double-exponential fit; τ_{recov}, single-exponential recovery fit for currents measured with a two-pulse protocol (steps from −100 to +40 mV); *$P < 0.05$, unpaired *t*-test; #, data from siDPPX day 2 only.

cell recording because current levels in patches were too small on average to compare between groups. We showed previously that this window current is produced by Kv4-containing channels and has a major influence on subthreshold excitability in CA1 neurons, acting as a voltage shunt to determine the subsequent activation of other voltage-dependent conductances (Kim et al. 2005).

Also consistent with experiments in heterologous systems, we observed siDPPX to cause a decrease in the rate of inactivation at low voltages (from 20.1 ± 1.7 ms for control to 29.6 ± 3.7 ms for siDPPX at −20 mV, Table 1) and recovery from inactivation (from 19.0 ± 1.5 ms for control to 31.8 ± 6.6 in siDPPX-expressing neurons 2 days after infection, Table 1). Such changes in gating speeds could follow shifts in voltage dependence.

Opposing sub- and suprathreshold effects of DPPX on CA1 excitability

SUBTHRESHOLD EFFECTS. Based on voltage-clamp results from heterologous expression studies showing a large depolarizing shift in the A-current activation curve, we expected siDPPX knockdown to enhance cellular excitability. However, our experimental observations in current-clamp recordings (presented in Figs. 3 and 4) showed the opposite, a *decrease* in excitability. Consistent with our whole cell voltage-clamp measurements shown in Fig. 2, our current-clamp findings suggest the presence of a larger A-current near resting potentials on DPPX knockdown compared with control. We suggest, with support from computer simulations (Fig. 5), that this unexpected result is at least partially attributable to the under appreciation of the effect DPPX has on the *slope* of the activation curve.

For current-clamp experiments, we delivered a series of current injections, from −200 to +350 pA in 50-pA increments, in whole cell recordings of siRNA (siDPPX or negative control siRNA)-expressing CA1 pyramidal neurons, 1–3 days postinfection. In Fig. 3, we show that, on subthreshold current injection from −60 mV, both the peak and steady-state voltage deflections are reduced 2 days after siDPPX expression. No such decrease is observed 1 day after siDPPX infection. This finding is again consistent with our previous results showing a window current in CA1 pyramidal neurons that affects input resistance (Kim et al. 2005). In that previous study, we showed that this current is Kv4-mediated as it was reduced on expression of a Kv4-dominant negative mutation and enhanced with Kv4.2 overexpression. From Fig. 3, *A* and *C,* it is apparent that the "sag" between peak and steady-state voltages are different

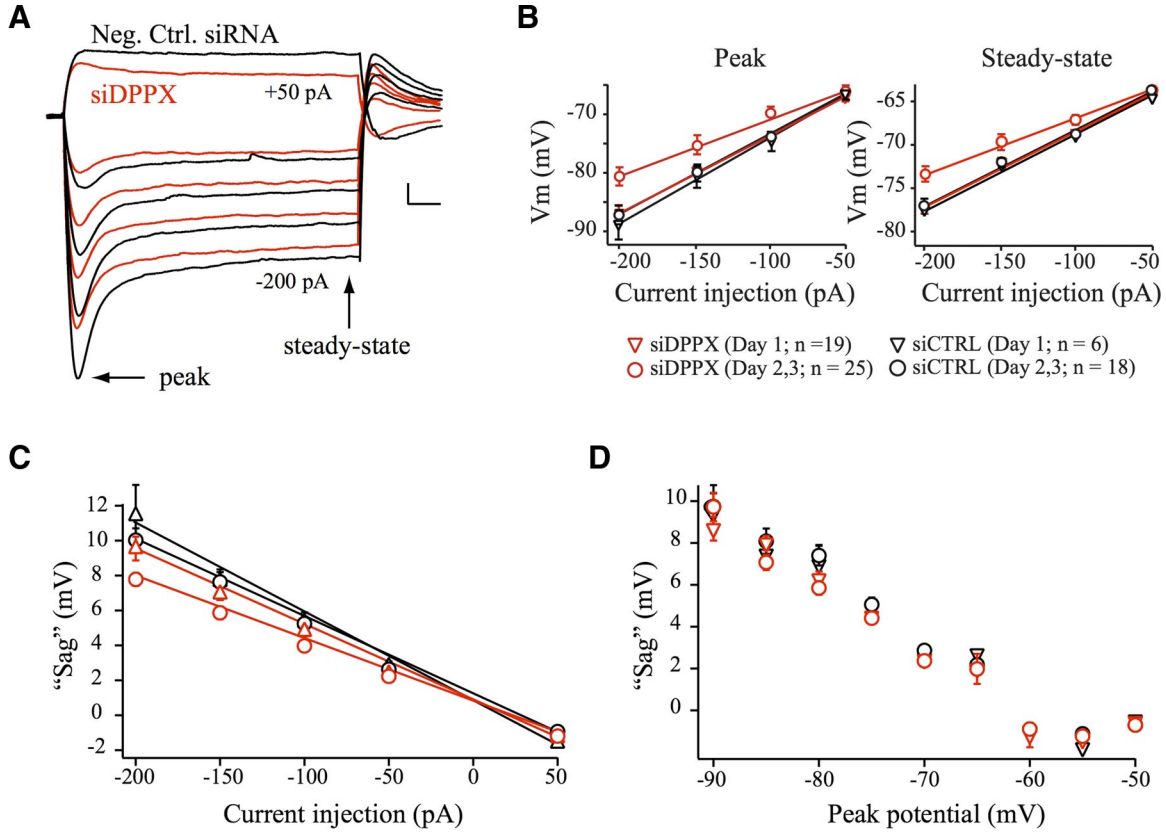

FIG. 3. DPPX knockdown decreases CA1 input resistance. *A*: subthreshold voltage transients generated in response to 900-ms current injections for siDPPX (red traces) and control neurons (black traces) recorded 2 days after infection. Current injections were −200, −150, −100, −50, and +50 pA. Smaller voltage deflections are seen in the siDPPX cell for all injections. *B*: current-voltage relationship for the peak (*left*) and steady-state (~900 ms, *right*) voltages for negative control siRNA-expressing cells (black symbols) and siDPPX-expressing cells (red symbols). Lines are linear regression fits of the data. Both peak and steady-state responses are reduced compared with control in siDPPX-expressing neurons after 2 days postinfection (day 2–3, red circles) but not 1 day postinfection (day 1, red triangles). *C*: plot showing the "sag" (difference between peak and steady-state voltages) for each current injection. On hyperpolarization, less sag is seen for siDPPX on after day 2 indicating less I_h activation. *D*: sag is plotted against the peak voltage. This relationship did not differ between experimental groups indicating that the changes in I_h seen in *C* are due to siDPPX-dependent reduction in the peak voltage reached early during the current injection. Error bars represent SE.

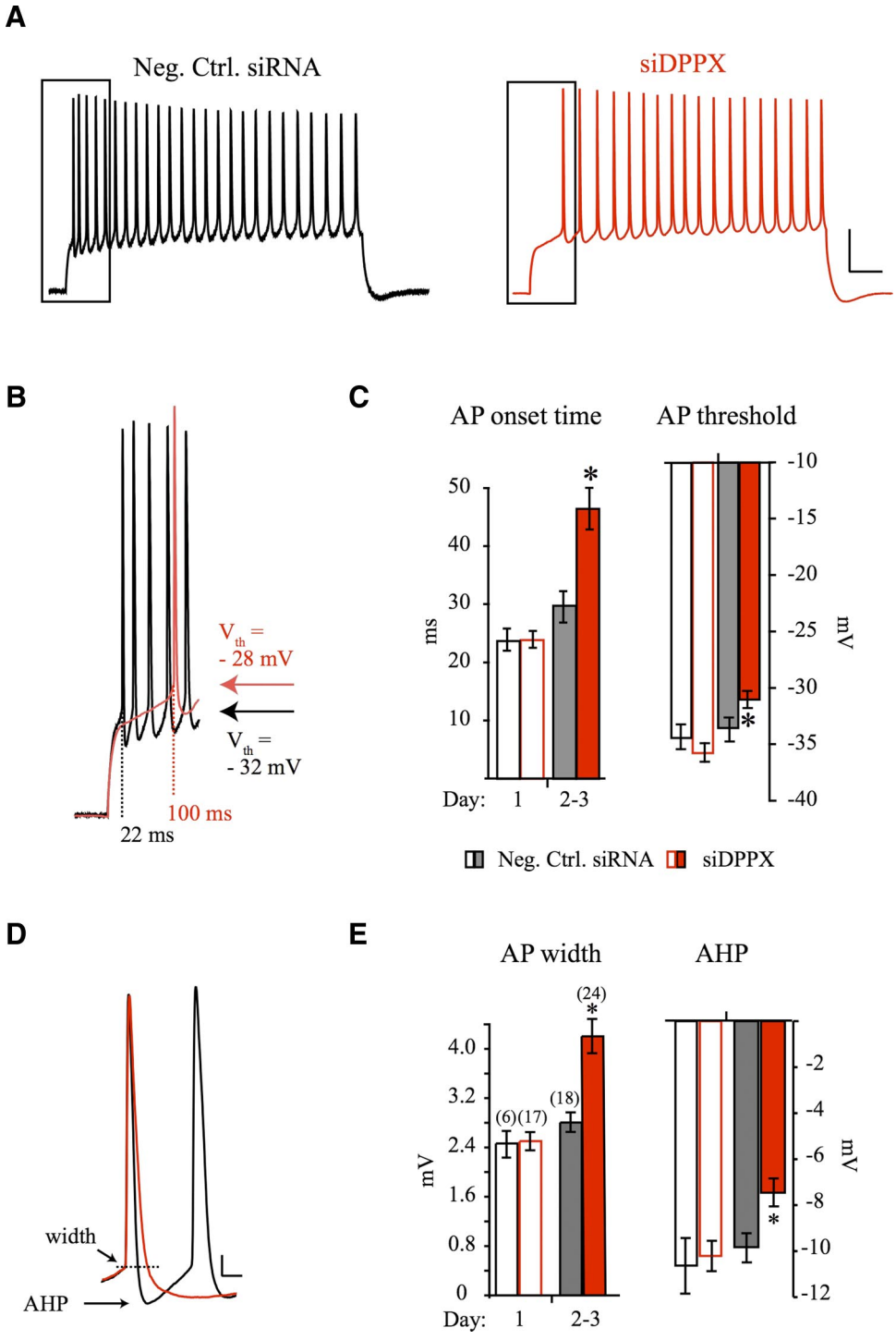

FIG. 4. DPPX regulates the excitability of CA1 pyramidal neurons. *A*: traces recorded on suprathreshold, 300 pA, current injection in siDPPX (red traces) and negative control siRNA-expressing neurons (black traces). Rectangles indicate portion of the traces shown in *B*. *B*: enlarged and overlapped traces from *A* show siDPPX-expressing neurons (red trace) have a delayed onset and higher voltage threshold for the 1st action potential (AP) on step-current injection compared with negative control siRNA-expressing neurons (black trace). *C*: pooled AP onset and threshold data for siDPPX (red bars) and negative control siRNA-expressing neurons (gray bars). One day postinfection (open bars), no difference in either onset or threshold is observed between experimental groups. However, both onset and threshold are affected by siDPPX expression beginning 2 days postinfection (filled bars). Threshold data are measured from ramp current injections (Kim et al. 2005). Asterisks indicates $P < 0.05$. Error bars represent SE. *D*: broadened and aligned traces from *A* to show that the 1st AP initiated in siDPPX-expressing neurons (red trace) are broader with weaker afterhyperpolarization compared with negative control siRNA-expressing neurons (black trace). *E*: pooled AP width and afterhyperpolarization (AHP) data for siDPPX (red bars) and negative control siRNA-expressing neurons (gray bars). One day postinfection (open bars), no difference in either width or AHP is observed between experimental groups. However, both are affected by siDPPX expression beginning 2 days postinfection (filled bars). Numbers in parentheses are the "*n*" number for data in *C* and *E*. Asterisks indicates $P < 0.05$. Error bars represent SE.

between experimental groups, suggesting a change in the hyperpolarization activated current, I_h (Pape 1996). However, in Fig. 3*D* we show that, for a given peak voltage, the absolute value of this sag is preserved between experimental groups, indicating that there is no change in I_h conductance. Bath application of the I_h blocker ZD7288 (20 μM) nearly tripled input resistances in both siDPPX and negative control siRNA-expressing neurons (siDPPX, 70.4 ± 4.9 MΩ, $n = 25$; siDPPX + ZD288, 231.6 ± 10.2 MΩ, $n = 14$; negative control, 79.8 ± 5.1 MΩ, $n = 18$; negative control + ZD288, 233.6 ± 12.5 MΩ, $n = 12$; all recordings 2–3 days postinfection). This large change in input resistance with I_h block made it difficult to determine if a smaller difference between siDPPX and control siRNA-expressing neurons remained. We show in the following text, however, that I_h block does not eliminate siDPPX-mediated, depolarization-induced changes in AP firing (i.e., AP threshold and onset time).

From the data in Fig. 3, along with our immunoblot data showing no effects of siDPPX on the expression of other endogenous ion channels, including HCN channels, (Supplemental Fig. S3), we conclude that the Kv4-mediated changes in resting conductance leads to changes in the activity (activation/

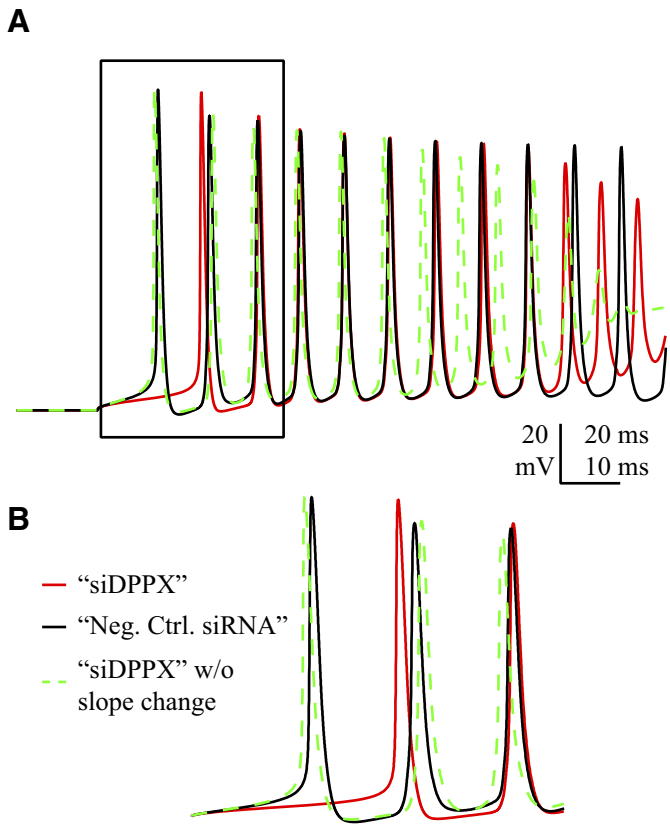

FIG. 5. NEURON simulations reveal how individual kinetic changes to A currents caused by DPPX contribute to specific firing properties of hippocampal CA1 neurons. Traces from NEURON simulations incorporating control (black trace) and siDPPX (red trace) A-channel properties. From the control simulation to the DPPX siRNA simulation, onset of the 1st AP increased from 17.9 to 30.2 ms. In addition, the peak amplitude of the 1st AP decreased from 108.4 to 107.2 mV, the 1st AP afterhyperpolarization potential decreased from −1.4 to −0.4 mV, and the 1st AP half-width increased from 1.9 to 2.0 ms. No change in frequency was found after the 1st few APs. These findings are all consistent with experimental results. Traces in *A* are expanded in *B*.

inactivation/deactivation) of other voltage-dependent currents (most significantly I_h for these data, given its prominent role in setting resting membrane resistance) but that there is no evidence for compensatory changes in the channel expression or conductance of this or other types of voltage-gated channels.

We have previously shown that the Kv4-mediated subthreshold current affects AP onset time and threshold in CA1 pyramidal neurons from organotypic slice cultures (Kim et al. 2005). Here we show that this current is strengthened *at subthreshold potentials* in siDPPX-expressing neurons through the depolarizing inactivation curve shift and activation curve slope change (Fig. 2) and, accordingly, that knockdown of DPPX results in a delayed AP onset and increased threshold on suprathreshold current injection (Fig. 4, *A–C*). As with the siDPPX effect on input resistance, the changes in AP onset and threshold were not observed until 2 days after infection (Fig. 4*C*).

These current-clamp results do not, however, necessarily reflect an isolated effect of siDPPX on A-type currents. Rather, as noted in the preceding text, it is likely that the enhanced subthreshold A current in siDPPX-expressing neurons leads to changes in activation/inactivation of other voltage-dependent subthreshold currents. For example, siDPPX-enhanced A currents opposing depolarization would be expected to decrease Na^+ channel activity, which could contribute to the delayed AP onset and increased threshold presented in Fig. 4, *A–C*. However, unlike for input resistance (Fig. 3), I_h does not significantly contribute to AP onset time or threshold in these experiments as differences between siDPPX and control recordings persisted in the presence of ZD7288 (20 μM; AP onset: siDPPX, 48.2 ± 4.5 ms, $n = 12$; control, 33.2 ± 5.1 ms, $n = 12$, $P < 0.5$; AP threshold: siDPPX, −29.6 ± 0.6 ms, $n = 14$; control, −32.4 ± 1.0 ms, $n = 12$, $P < 0.5$; all recordings 2–3 days postinfection, data not shown).

SUPRATHRESHOLD EFFECTS. Although, as a result of siDPPX treatment, the A current is enhanced at subthreshold voltages, leading to a decrease in excitability, on AP initiation, the right-shifted activation curve in siDPPX-expressing neurons results in less A-current activation at suprathreshold voltages. The reduced suprathreshold A-current results in weaker AP repolarization (Fig. 4, *D* and *E*). One day postinfection (day 1) no difference in AP width was observed between siDPPX-expressing and control siRNA-expressing neurons. However, APs in siDPPX-expressing neurons broadened after day 2, whereas no change was observed in control neurons (Fig. 4, *D* and *E*). As previously observed after A-current downregulation with Kv4.2 dominant negative expression, (Kim et al. 2005), weakened repolarization resulted in smaller after-hyperpolarization potentials (AHPs, Fig. 4, *D* and *E*).

We observed in our current-clamp recordings a slight decrease in firing frequency in siDPPX-expressing neurons over the first 100 ms of current injection (from 49.0 ± 1.3 Hz, $n = 18$ in control to 43.4 ± 1.0 Hz, $n = 24$ for siDPPX, 2–3 days postinfection, $P < 0.05$, data not shown). Over this time period, average AP amplitude was also slightly decreased (from 94.0 ± 0.9 to 91.4 ± 0.9 mV for control and siDPPX groups, respectively, $P < 0.05$, data not shown). The smaller peak AP amplitude, activating fewer K^+ channels would also be expected to contribute to the weaker AP repolarization shown in Fig. 4*D*. For the remainder of the current injection (100–900 ms), no difference between groups was observed in frequency or amplitude.

Together, the current-clamp data show that DPPX acts to sharpen neuronal signaling. At subthreshold potentials, DPPX reduces I_A through its effect on steady-state inactivation and on the voltage slope for activation. Although this change in current at subthreshold voltages appears small in magnitude (Fig. 2), it may have considerable consequences for neuronal excitably by influencing the activity of other voltage-gated channels. Once an AP is initiated, however, the left-shifted activation curve by DPPX has the opposite effect, enhancing I_A to decrease neuronal excitability by speeding up repolarization and enhancing signal precision.

Computer simulations

To gain an appreciation for how individual kinetic changes to A currents caused by DPPX contribute to specific firing properties of hippocampal CA1 neurons (AP onset time, threshold, peak, repolarization, and firing rates), we used a simple compartmental model in the NEURON programming environment of a hippocampal CA1 neuron with Hodgkin-Huxley-like voltage-gated Na^+ conductances, rapidly inactivating A-type K^+ conductances, noninactivating delayed-rec-

tifier K^+ conductances, and a voltage-independent leak current. The morphology of the dendrites and soma of this computation CA1 neuron were taken from a previous simulation and is morphologically realistic (Migliore et al. 1999).

We created two implementations of the model, one for simulating siDPPX-expressing neurons and one for simulating control neurons. The two implementations were identical except that in the DPPX knockdown case, we incorporated the experimentally-observed voltage-dependent changes to A-type K^+ currents with siDPPX causing a rightward shift in both the steady-steady inactivation (from $V_h = -69$ in control to $V_h = -64$ for siDPPX) and activation curves (from $V_h = -9$ in control to $V_h = +3$ for siDPPX) and a shallowing of the slope of the steady-state activation curve (from $k = 18$ in control to $k = 23$ for siDPPX). With these modifications to the A-type K^+ conductances, we were then able to reproduce the experimentally observed results in changes to the whole cell firing properties of neurons. Specifically, we observed the following changes in the DPPX knockdown model (Fig. 5, "siDPPX") compared with the control model ("Neg. Ctrl siRNA"): threshold decreased from −42.5 to −38 mV, onset time of the first AP increased from 17.3 to 28.8 ms, firing frequency decreased from 76.8 to 73.4 Hz, peak amplitude of the first AP decreased from 108.4 to 107.1 mV, first AP afterhyperpolarization potential decreased from −2.4 to −0.6 mV, and first AP half-width increased from 1.6 to 2.0 ms; all consistent with experimental results (Fig. 4).

We next investigated the individual effects of the activation and inactivation curve shifts to understand more clearly the nonlinear interactions between the two. To do so, we plotted onset time of the first AP, firing frequency, half-width at half-max of the first AP, and afterhyperpolarization potential of the first AP as functions of both activation and inactivation curves midpoints. The results are presented in Supplemental Fig. S4. We found that, in general, rightward shifts in the activation and inactivation curves produced opposite effects. Specifically, a rightward shift in inactivation curve (increasing the number of channels available for activation), increased AP onset time, decreased AP peak and accelerated AP repolarization (narrower APs with larger AHPs). No effect of the inactivation curve shift was found for frequency. Conversely, a rightward shift in the activation curve (which tends to decrease the open-state probability of the channel) decreased AP onset time and increased AP peak but had no clear effect on AP repolarization or frequency. The siDPPX-mediated change in activation curve slope had its greatest effect subthreshold, determining AP onset ("both" in Supplemental Fig. S4) times. In summary of our computer simulations, we verified that all three changes between control and siDPPX neurons, rightward shifts in both the steady-state activation and inactivation and a shallowing of the slope of the steady-state activation curve, were individually necessary to explain the changes in whole cell firing properties.

DPPX sharpens AP signaling

We conclude that an important physiological role for DPPX is to increase CA1 responsiveness to stimulation by decreasing the proportion of A-channels active at subthreshold voltages. This result is achieved by hyperpolarizing the A-current inactivation curve and by sharpening activation with a steeper conductance-voltage activation slope. Less A-current active subthreshold will also enhance Na^+ channel activity on depolarization, further enhancing excitability. Suprathreshold, the left-shifted A-channel activation curve leads to narrower APs and larger AHPs. These two opposing (sub- and suprathreshold) results of DPPX expression are offsetting in regard to frequency but suggest that both the rise and fall of the first AP initiated on stimulation will be boosted by DPPX and thus sluggish in siDPPX neurons compared with control.

Accordingly, we analyzed the rate of rise and fall for the first AP for each group on a 300-pA current injection (Fig. 6). As predicted, the maximal rate of both AP rise and fall are reduced by siDPPX expression (2–3 days postinfection; max. dV/dt rise: 178 ± 12, $n = 22$ and 141 ± 11, $n = 26$; max. dV/dt fall: −43 ± 3.3 and −33.7 ± 2.8 for control and siDPPX, respectively). No difference between groups was found 1 day postinfection. The relative sluggishness of AP kinetics in siDPPX-expressing neurons is perhaps best demonstrated by the phase-plane plot shown in Fig. 6*B*. The phase-plane plot captures the AP threshold increase for the siDPPX recordings (red traces) along with the decrease in maximal AP rise and fall compared with control (black traces).

DISCUSSION

We have used a viral delivery system to introduce siRNA targeting DPPX (siDPPX), an auxiliary subunit of a prominent family of K^+ channels in CA1 neurons of organotypic slice culture. Our results support a role of DPPX in regulating a number of biophysical features of CA1 A-type currents. With the aid of NEURON simulations where individual A-current properties were systematically changed, we link the measured channel modifications to the changes in AP shape and firing patterns we observed in CA1 neurons expressing siDPPX. We conclude that relatively small changes in the voltage-dependence of A-current activity imparted by DPPX play a critical role in regulating the excitability of CA1 pyramidal neurons. Interestingly, the particular ways in which A currents are modulated by DPPX lead to opposite effects *sub-* and *suprathreshold* that work in concert to improve neuronal responsiveness and enhance signal precision.

Effects of DPPX knockdown on CA1 A-type currents

A number of previous studies in heterologous expression systems have shown modulation of Kv4 channel voltage-dependent properties by DPPX or its related family member DPP10 (Dougherty and Covarrubias 2006; Jerng et al. 2004b, 2005; Nadal et al. 2003, 2006; Ren et al. 2005; Zagha et al. 2005). Common among these are DPPL-mediated modulation of Kv4 channel voltage-dependent activation and steady-state inactivation, faster kinetics, and enhanced membrane surface expression. CA1 pyramidal cells express only one of the two DPPL genes known (DPPX) (Zagha et al. 2005) and hence elimination of only DPPX should affect these parameters. We report here data consistent with most of these changes on knockdown of DPPX for native A-type currents in hippocampal CA1 pyramidal neurons. In accordance with data from expression systems, neurons expressing siRNA-targeting DPPX exhibited changes in the voltage-dependence of A-current

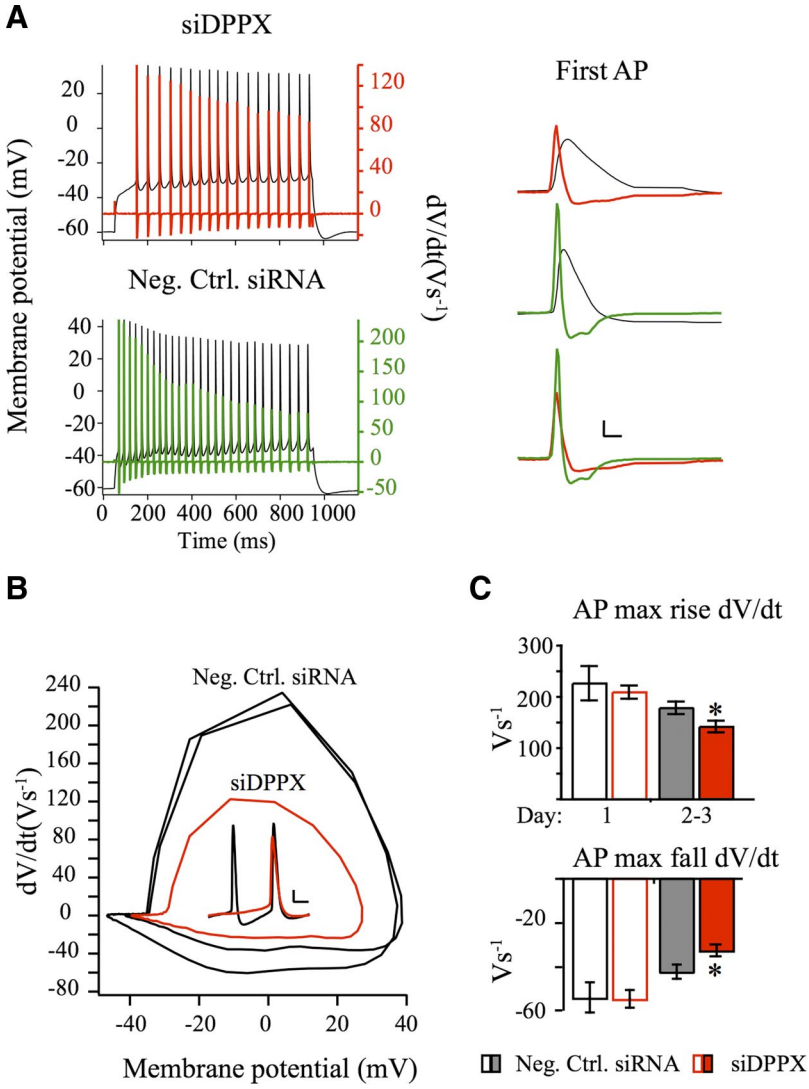

FIG. 6. DPPX siRNA weakens both the rate of rise and fall of action potentials in hippocampal CA1 neurons. *A*: examples traces of AP firing in DPPX siRNA (*top*) and negative control siRNA (*bottom*)-expressing CA1 pyramidal neurons (black traces). Overlaid are the 1st temporal derivatives showing reduced peak rates of rise and fall for DPPX siRNA-expressing neurons (DPPX siRNA in red, control siRNA in green). Traces to the right show the 1st AP aligned with its derivative. The bottom set of traces show the overlaid 1st derivatives for DPPX siRNA (red trace) and negative control siRNA (green trace). *B*: phase-plane plot of the action potentials shown in the *inset* for DPPX siRNA (red traces) and control siRNA (black traces). *C*: pooled data showing a significant reduction in both rates of rise and fall for APs in DPPX siRNA-expressing neurons 2–3 days after infection compared with control siRNA (*, $P < 0.05$, unpaired *t*-test). No differences were observed 1 day after infection. Error bars represent SE.

gating, with a larger effect on activation than on inactivation. In addition, the kinetics of A-current activation, inactivation, and recovery from inactivation were affected in siDPPX-expressing neurons in a fashion consistent with the reported effects of DPPX on Kv4 currents.

In heterologous cells, DPPX (and DPP10) significantly accelerate the rate of inactivation of Kv4 channels (Amarillo et al. 2008; Jerng et al. 2005, 2007; Nadal et al. 2003; Zagha et al. 2005). It is believed that the somatodendritic A current is composed of Kv4 encoded channels in a ternary complex with DPPX and KChIP auxiliary subunits (Jerng et al. 2005; Kim et al. 2005). When heterologous cells are transfected with both KChIP and DPPX, the accelerating effect of DPPX is largely reduced (Amarillo et al. 2008; Jerng et al. 2007; Nadal et al. 2003) and is mainly observed in the negative voltage range (between −60 and −10 mV). We found no significant decrease in A-current inactivation rate in outside-out patches at high voltages (+40 mV, 31.1 ± 2.9 ms, $n = 26$ for siDPPX vs. 33.9 ± 3.7 ms, $n = 23$ for negative controls siRNA, weighted sum of 2 exponentials; $P > 0.05$; Table 1). However, we found siDPPX reduced the rate of A-current inactivation at negative potentials in outside-out patches (−20 mV, Table 1). This is what would be expected if the native CA1 Kv4 channels normally contain both KChIPs and DPPX and only KChIPs on treatment with siDPPX.

Ternary channels containing Kv4.2, KChIP, and DPPX expressed in heterologous cells have rates of inactivation that slow down with increasing depolarization (Amarillo et al. 2008; Jerng et al. 2005, 2007; Kaulin et al. 2007). This unique voltage dependence stems from a preference for closed-over open-state inactivation, a trait apparently promoted by the sequestration of the N-terminal inactivation gate by KChIP (Amarillo et al. 2008; Beck et al. 2002; Jerng et al. 2005, 2007; Kaulin et al. 2007; Pioletti et al. 2006; Wang et al. 2007) and is not found for Kv4.2 channels in complex solely with DPPX. Furthermore, Amarillo et al. (2008) observed that the voltage range over which the rate of inactivation decreases with increasing depolarization is broadened when DPPX is present in addition to KChIP. The time constants of inactivation of the native CA1 A-current also increase with depolarization in a voltage range that is similar to that observed for Kv4.2 channels in the presence of KChIP and DPPX (Hoffman et al. 1997), further supporting the notion that the native current in CA1 neurons contains both accessory subunits.

Notably different from studies in expression systems, however, we did not observe significant changes in the peak

A-current levels. In addition to DPPLs, Kv4 currents are enhanced by co-expression with KChIPs, the other major class of Kv4 auxiliary subunits (An et al. 2000; Shibata et al. 2003). KChIP binding to Kv4 may enhance surface expression through a redundant mechanism as DPPX, perhaps by preventing access to a Kv4 N-terminal ER retention domain (Jerng et al. 2004a). Also it was been shown that constitutively active CaMKII enhances A-current expression levels in CA1 neurons, decreasing cell excitability (Varga et al. 2004). This enhancement, if through direct phosphorylation of Kv4- or KchIP-containing channels in CA1 neurons might also remain unaffected by siDPPX expression.

Electrophysiological recordings (Chen et al. 2006; Hoffman et al. 1997; Yuan et al. 2002) show an increasing gradient of A-type current along CA1 hippocampal dendrites with distance from the soma, and we have recently reported the activity-dependent trafficking of Kv4.2 in CA1 pyramidal neurons (Kim et al. 2007). In this study, Kv4.2 channels were rapidly internalized, and A-currents decreased, on stimulation in an NMDA-dependent manner. There exist then a number of factors controlling A-channel expression in CA1 neurons. Nonetheless our findings suggest that DPPX is not necessary for functional expression in CA1 pyramidal neuron somata. However, from these somatic recordings, we cannot exclude the possibility that DPPX may affect membrane surface stability of Kv4.2 channels in dendrites.

Effects of DPPX knockdown on hippocampal CA1 signaling

The primary conclusion from our current-clamp studies is that siDPPX expression causes an unexpected decrease in subthreshold excitability in CA1 pyramidal neurons, suggesting that DPPX natively enhances neuronal response to stimulation. Based on data from heterologous expression studies showing DPPX co-expression with Kv4 subunits leads to enhanced A-current amplitudes, a large hyperpolarizing activation curve shift, faster activation, and recovery from inactivation kinetics, we expected a role of DPPX in enhancing A-type K^+ activity, decreasing cell excitability. Knockdown of DPPX was therefore predicted to enhance excitability.

Our modeling data suggest two explanations for this unanticipated finding. First, the depolarizing inactivation curve shift produced by siDPPX expression leaves more channels available for activation at rest, delaying AP onset. Although smaller in magnitude than the activation curve shift, the relative steepness of the inactivation curve for A-type currents in CA1 neurons (no change in inactivation curve slope was found for siDPPX expression, Fig. 2) allows for even a small shift to have a large physiological effect. From Fig. 2, ~27% of maximal A currents are available for activation at −60 mV, near rest in control siRNA-expressing neurons compared with ~39% in siDPPX expressing. Second, we find a significant shallowing of the voltage dependence of activation gating in siDPPX expression neurons compared with control. This modification, together with the inactivation curve shift, actually enhanced the proportion of channels activated at subthreshold potentials despite the depolarizing shift measured for the half-activation voltage (Fig. 2), a finding supported by our current-clamp result showing a decreased input resistance in siDPPX-expressing neurons (Fig. 3) and delayed AP onset (Fig. 4). Our neuron simulations suggest that this change in slope has a particularly strong effect on AP onset times (Fig. 5). We suggest that enhancing subthreshold I_A may delay Na^+ channel activation to influence AP onset times.

Generalized function of DPPX in CA1 neurons

Taken together, our results suggest that DPPX acts to boost neuronal response in CA1 pyramidal neurons of the hippocampus. By decreasing subthreshold A currents and steepening the voltage dependence of A-channel activation, DPPX decreases AP delay on stimulation and sharpens its rise. However, after initiation, DPPX acts to accelerate repolarization to enhance the precision of signaling. Although it has been commonly thought that neurons represent information through mean firing rate, spike timing as an encoding mechanism has recently been observed in sensory systems (VanRullen et al. 2005). In the hippocampus too, the precision timing of APs is important for spike-timing-dependent plasticity and phase firing during theta oscillation. A-type K^+ currents may then be dynamically regulated by auxiliary subunit co-expression (e.g., "tuned-up" by DPPX) in different neuron types or in the same neuron under different activity levels or in microdomains.

The results reported here were all obtained from somatic recordings. It is likely that the effect of DPPX co-expression, should it occur, will be even more pronounced in the apical dendrites of CA1 neurons where A-current density is increased, modulating back-propagating AP amplitude, opposing AP initiation and shaping synaptic inputs and integration (Cai et al. 2004; Chen et al. 2006; Golding et al. 1999; Hoffman et al. 1997; Kim et al. 2005, 2007; Losonczy and Magee 2006; Ramakers and Storm 2002; Watanabe et al. 2002; Yuan et al. 2002). Our results predict that DPPX would predominately act to enhance dendritic excitability by reducing subthreshold A-channel activity. However, the DPPX-mediated hyperpolarization of A-channel activation may act as a safety factor to counter depolarization during coordinated or intense stimulation and burst firing.

ACKNOWLEDGMENTS

We thank members of Drs. Richard Aldrich and Dan Johnston's labs for a critical review of versions of this manuscript, Dr. Dane Chetkovich for supplying HCN antibodies, and D. Medrano-Velasquez for technical support.

Present address of J. Kim: Janelia Farm Research Campus, Howard Hughes Medical Institute, 19700 Helix Dr., Ashburn, VA 20147.

GRANTS

This work was supported by the National Institute of Child Health and Human Development Intramural Research Program and by National Institute of Neurological Disorders and Stroke Grants NS-30989 and NS-045217 and National Science Foundation Grant IBN-0314645 to B. Rudy.

REFERENCES

Amarillo Y, De Santiago-Castillo JA, Dougherty K, Kwon E, Covarrubias M, Rudy B. Ternary Kv4.2 channels recapitulate voltage-dependent inactivation kinetics of A-type K^+ channels in cerebellar granule neurons. *J Physiol* 586: 2093–2106, 2008.

An WF, Bowlby MR, Betty M, Cao J, Ling HP, Mendoza G, Hinson JW, Mattsson KI, Strassle BW, Trimmer JS, Rhodes KJ. Modulation of A-type potassium channels by a family of calcium sensors. *Nature* 403: 553–556, 2000.

Beck EJ, Bowlby M, An WF, Rhodes KJ, Covarrubias M. Remodelling inactivation gating of Kv4 channels by KChIP1, a small-molecular-weight calcium-binding protein. *J Physiol* 538: 691–706, 2002.

Brummelkamp TR, Bernards R, Agami R. A system for stable expression of short interfering RNAs in mammalian cells. *Science* 296: 550–553, 2002.

Cai X, Liang CW, Muralidharan S, Kao JP, Tang CM, Thompson SM. Unique roles of SK and Kv4.2 potassium channels in dendritic integration. *Neuron* 44: 351–364, 2004.

Chen X, Yuan LL, Zhao C, Birnbaum SG, Frick A, Jung WE, Schwarz TL, Sweatt JD, Johnston D. Deletion of Kv4.2 gene eliminates dendritic A-type K^+ current and enhances induction of long-term potentiation in hippocampal CA1 pyramidal neurons. *J Neurosci* 26: 12143–12151, 2006.

Colbert CM, Magee JC, Hoffman DA, Johnston D. Slow recovery from inactivation of Na^+ channels underlies the activity-dependent attenuation of dendritic action potentials in hippocampal CA1 pyramidal neurons. *J Neurosci* 17: 6512–6521, 1997.

Connor JA, Stevens CF. Prediction of repetitive firing behaviour from voltage clamp data on an isolated neurone soma. *J Physiol* 213: 31–53, 1971.

Dougherty K, Covarrubias M. A dipeptidyl aminopeptidase-like protein remodels gating charge dynamics in Kv4.2 channels. *J Gen Physiol* 128: 745–753, 2006.

Golding NL, Jung HY, Mickus T, Spruston N. Dendritic calcium spike initiation and repolarization are controlled by distinct potassium channel subtypes in CA1 pyramidal neurons. *J Neurosci* 19: 8789–8798, 1999.

Hines ML, Carnevale NT. The NEURON simulation environment. *Neural Comput* 9: 1179–1209, 1997.

Hoffman DA, Magee JC, Colbert CM, Johnston D. K^+ channel regulation of signal propagation in dendrites of hippocampal pyramidal neurons. *Nature* 387: 869–875, 1997.

Holmes WR. The role of dendritic diameters in maximizing the effectiveness of synaptic inputs. *Brain Res* 478: 127–137, 1989.

Jagla B, Aulner N, Kelly PD, Song D, Volchuk A, Zatorski A, Shum D, Mayer T, De Angelis DA, Ouerfelli O, Rutishauser U, Rothman JE. Sequence characteristics of functional siRNAs. *RNA* 11: 864–872, 2005.

Jerng HH, Kunjilwar K, Pfaffinger PJ. Multiprotein assembly of Kv4.2, KChIP3 and DPP10 produces ternary channel complexes with ISA-like properties. *J Physiol* 568: 767–788, 2005.

Jerng HH, Lauver AD, Pfaffinger PJ. DPP10 splice variants are localized in distinct neuronal populations and act to differentially regulate the inactivation properties of Kv4-based ion channels. *Mol Cell Neurosci* 35: 604–624, 2007.

Jerng HH, Pfaffinger PJ, Covarrubias M. Molecular physiology and modulation of somatodendritic A-type potassium channels. *Mol Cell Neurosci* 27: 343–369, 2004a.

Jerng HH, Qian Y, Pfaffinger PJ. Modulation of Kv4.2 channel expression and gating by dipeptidyl peptidase 10 (DPP10). *Biophys J* 87: 2380–2396, 2004b.

Johnston D, Hoffman DA, Colbert CM, Magee JC. Regulation of back-propagating action potentials in hippocampal neurons. *Curr Opin Neurobiol* 9: 288–292, 1999.

Johnston D, Hoffman DA, Magee JC, Poolos NP, Watanabe S, Colbert CM, Migliore M. Dendritic potassium channels in hippocampal pyramidal neurons. *J Physiol* 525: 75–81, 2000.

Jung HY, Mickus T, Spruston N. Prolonged sodium channel inactivation contributes to dendritic action potential attenuation in hippocampal pyramidal neurons. *J Neurosci* 17: 6639–6646, 1997.

Kaulin Y, De Santiago-Castillo JA, Rocha C, Covarrubias M. Mechanism of the modulation of Kv4:KChIP-1 channels by external K^+. *Biophys J* 94: 1241–1251, 2008.

Kim J, Dittgen T, Nimmerjahn A, Waters J, Pawlak V, Helmchen F, Schlesinger S, Seeburg PH, Osten P. Sindbis vector SINrep(nsP2S726): a tool for rapid heterologous expression with attenuated cytotoxicity in neurons. *J Neurosci Methods* 133: 81–90, 2004.

Kim J, Hoffman DA. Potassium channels: newly found players in synaptic plasticity. *Neuroscientist* 14: 276–286, 2008.

Kim J, Jung SC, Clemens AM, Petralia RS, Hoffman DA. Regulation of dendritic excitability by activity-dependent trafficking of the a-type k(+) channel subunit kv4.2 in hippocampal neurons. *Neuron* 54: 933–947, 2007.

Kim J, Wei DS, Hoffman DA. Kv4 potassium channel subunits control action potential repolarization and frequency-dependent broadening in rat hippocampal CA1 pyramidal neurones. *J Physiol* 569: 41–57, 2005.

Kin Y, Misumi Y, Ikehara Y. Biosynthesis and characterization of the brain-specific membrane protein DPPX, a dipeptidyl peptidase IV-related protein. *J Biochem* 129: 289–295, 2001.

Lauver A, Yuan LL, Jeromin A, Nadin BM, Rodriguez JJ, Davies HA, Stewart MG, Wu GY, Pfaffinger PJ. Manipulating Kv4.2 identifies a specific component of hippocampal pyramidal neuron A-current that depends upon Kv4.2 expression. *J Neurochem* 99: 1207–1223, 2006.

Losonczy A, Magee JC. Integrative properties of radial oblique dendrites in hippocampal CA1 pyramidal neurons. *Neuron* 50: 291–307, 2006.

Magee JC, Cook EP. Somatic EPSP amplitude is independent of synapse location in hippocampal pyramidal neurons. *Nat Neurosci* 3: 895–903, 2000.

Migliore M, Hoffman DA, Magee JC, Johnston D. Role of an A-type K^+ conductance in the back-propagation of action potentials in the dendrites of hippocampal pyramidal neurons. *J Comput Neurosci* 7: 5–15, 1999.

Nadal MS, Amarillo Y, Vega-Saenz de Miera E, Rudy B. Evidence for the presence of a novel Kv4-mediated A-type K(+) channel-modifying factor. *J Physiol* 537: 801–809, 2001.

Nadal MS, Amarillo Y, Vega-Saenz de Miera E, Rudy B. Differential characterization of three alternative spliced isoforms of DPPX. *Brain Res* 1094: 1–12, 2006.

Nadal MS, Ozaita A, Amarillo Y, Vega-Saenz de Miera E, Ma Y, Mo W, Goldberg EM, Misumi Y, Ikehara Y, Neubert TA, Rudy B. The CD26-related dipeptidyl aminopeptidase-like protein DPPX is a critical component of neuronal A-type K^+ channels. *Neuron* 37: 449–461, 2003.

Pape HC. Queer current and pacemaker: the hyperpolarization-activated cation current in neurons. *Annu Rev Physiol* 58: 299–327, 1996.

Pioletti M, Findeisen F, Hura GL, Minor DL Jr. Three-dimensional structure of the KChIP1-Kv4.3 T1 complex reveals a cross-shaped octamer. *Nat Struct Mol Biol* 13: 987–995, 2006.

Qi SY, Riviere PJ, Trojnar J, Junien JL, Akinsanya KO. Cloning and characterization of dipeptidyl peptidase 10, a new member of an emerging subgroup of serine proteases. *Biochem J* 373: 179–189, 2003.

Ramakers GM, Storm JF. A postsynaptic transient K(+) current modulated by arachidonic acid regulates synaptic integration and threshold for LTP induction in hippocampal pyramidal cells. *Proc Natl Acad Sci USA* 99: 10144–10149, 2002.

Ren X, Hayashi Y, Yoshimura N, Takimoto K. Transmembrane interaction mediates complex formation between peptidase homologues and Kv4 channels. *Mol Cell Neurosci* 29: 320–332, 2005.

Rhodes KJ, Carroll KI, Sung MA, Doliveira LC, Monaghan MM, Burke SL, Strassle BW, Buchwalder L, Menegola M, Cao J, An WF, Trimmer JS. KChIPs and Kv4 alpha subunits as integral components of A-type potassium channels in mammalian brain. *J Neurosci* 24: 7903–7915, 2004.

Schoppa NE, Westbrook GL. Regulation of synaptic timing in the olfactory bulb by an A-type potassium current. *Nat Neurosci* 2: 1106–1113, 1999.

Serodio P, Rudy B. Differential expression of Kv4 K^+ channel subunits mediating subthreshold transient K^+ (A-type) currents in rat brain. *J Neurophysiol* 79: 1081–1091, 1998.

Shibata R, Misonou H, Campomanes CR, Anderson AE, Schrader LA, Doliveira LC, Carroll KI, Sweatt JD, Rhodes KJ, Trimmer JS. A fundamental role for KChIPs in determining the molecular properties and trafficking of Kv4.2 potassium channels. *J Biol Chem* 278: 36445–36454, 2003.

Strop P, Bankovich AJ, Hansen KC, Garcia KC, Brunger AT. Structure of a human A-type potassium channel interacting protein DPPX, a member of the dipeptidyl aminopeptidase family. *J Mol Biol* 343: 1055–1065, 2004.

VanRullen R, Guyonneau R, Thorpe SJ. Spike times make sense. *Trends Neurosci* 28: 1–4, 2005.

Varga AW, Yuan LL, Anderson AE, Schrader LA, Wu GY, Gatchel JR, Johnston D, Sweatt JD. Calcium-calmodulin-dependent kinase II modulates Kv4.2 channel expression and upregulates neuronal A-type potassium currents. *J Neurosci* 24: 3643–3654, 2004.

Wang H, Yan Y, Liu Q, Huang Y, Shen Y, Chen L, Chen Y, Yang Q, Hao Q, Wang K, Chai J. Structural basis for modulation of Kv4 K^+ channels by auxiliary KChIP subunits. *Nat Neurosci* 10: 32–39, 2007.

Watanabe S, Hoffman DA, Migliore M, Johnston D. Dendritic K^+ channels contribute to spike-timing dependent long-term potentiation in hippocampal pyramidal neurons. *Proc Natl Acad Sci USA* 99: 8366–8371, 2002.

Yuan LL, Adams JP, Swank M, Sweatt JD, Johnston D. Protein kinase modulation of dendritic K^+ channels in hippocampus involves a mitogen-activated protein kinase pathway. *J Neurosci* 22: 4860–4868, 2002.

Zagha E, Ozaita A, Chang SY, Nadal MS, Lin U, Saganich MJ, McCormack T, Akinsanya KO, Qi SY, Rudy B. DPP10 modulates Kv4-mediated A-type potassium channels. *J Biol Chem* 280: 18853–18861, 2005.